Journal of the Endocrine Society, 2022, **6**, 1–11
https://doi.org/10.1210/jendso/bvac019
Advance access publication 10 February 2022
Clinical Research Article

Broadening the Spectrum of Loss-of-Function Variants in NPR-C-Related Extreme Tall Stature

Peter Lauffer,[1,*] Eveline Boudin,[2,*] Daniëlle C. M. van der Kaay,[3] Saskia Koene,[4] Arie van Haeringen,[4] Vera van Tellingen,[5] Wim Van Hul,[2] Timothy C. R. Prickett,[6] Geert Mortier,[2] Eric A. Espiner,[6,#] and Hermine A. van Duyvenvoorde[4,#]

[1]Department of Pediatric Endocrinology, Emma Children's Hospital, Amsterdam University Medical Center, 1105 AZ Amsterdam, the Netherlands
[2]Department of Medical Genetics, Antwerp University Hospital and University of Antwerp, 2650 Edegem, Belgium
[3]Department of Pediatric Endocrinology, Sophia Children's Hospital, Erasmus Medical Center, 3015 GD Rotterdam, the Netherlands
[4]Department of Clinical Genetics, Leiden University Medical Center, 2333 ZA Leiden, the Netherlands
[5]Department of Pediatrics, Catharina Hospital, 5623 EJ Eindhoven, the Netherlands
[6]Department of Medicine, University of Otago, 8140 Christchurch, New Zealand

*These authors share first authorship.
#These authors share last authorship.
Correspondence: Peter Lauffer MD, Emma Children's Hospital, Amsterdam University Medical Center, Department of Pediatric Endocrinology, Meibergdreef 9, 1105 AZ Amsterdam, the Netherlands. Email: p.lauffer@amsterdamumc.nl.

Abstract

Context: Natriuretic peptide receptor-C (NPR-C, encoded by *NPR3*) belongs to a family of cell membrane–integral proteins implicated in various physiological processes, including longitudinal bone growth. NPR-C acts as a clearance receptor of natriuretic peptides, including C-type natriuretic peptide (CNP), that stimulate the cGMP-forming guanylyl cyclase-coupled receptors NPR-A and NPR-B. Pathogenic variants in *CNP*, *NPR2*, and *NPR3* may cause a tall stature phenotype associated with macrodactyly of the halluces and epiphyseal dysplasia.

Objective: Here we report on a boy with 2 novel biallelic inactivating variants of *NPR3*.

Methods: History and clinical characteristics were collected. Biochemical indices of natriuretic peptide clearance and in vitro cellular localization of NPR-C were studied to investigate causality of the identified variants.

Results: We identified 2 novel compound heterozygous *NPR3* variants c.943G>A p.(Ala315Thr) and c.1294A>T p.(Ile432Phe) in a boy with tall stature and macrodactyly of the halluces. In silico analysis indicated decreased stability of NPR-C, presumably resulting in increased degradation or trafficking defects. Compared to other patients with NPR-C loss-of-function, the phenotype seemed to be milder: pseudo-epiphyses in hands and feet were absent, biochemical features were less severe, and there was some co-localization of p.(Ile432Phe) NPR-C with the cell membrane, as opposed to complete cytoplasmic retention.

Conclusion: With this report on a boy with tall stature and macrodactyly of the halluces we further broaden the genotypic and phenotypic spectrum of NPR-C-related tall stature.

Key Words: natriuretic peptide receptor-C, NPR3, natriuretic peptides, CNP, tall stature, macrodactyly

Abbreviations: ANP, atrial natriuretic peptide; BNP, brain natriuretic peptide; cGMP, cyclic guanosine monophosphate; CNP, C-type natriuretic peptide; GoF, gain of function; LoF, loss of function; NP, natriuretic peptide; NPR-C, natriuretic peptide receptor-C (NPR3).

Natriuretic peptide receptor-C (NPR-C or NPR3) is encoded by *NPR3* (MIM 108962). It belongs to the family of natriuretic peptide receptors, together with NPR-A (encoded by *NPR1*; MIM 108960) and NPR-B (encoded by *NPR2*; MIM 108961) [1]. NPR-A and NPR-B are highly homologous cell-surface receptors with an intracellular guanylyl cyclase moiety. Guanylyl cyclase catalyzes the conversion of guanosine triphosphate (GTP) to cyclic guanosine monophosphate (cGMP) upon binding of a ligand to the NPR-A or NPR-B receptors, including atrial natriuretic peptide (ANP; MIM 108780), brain natriuretic peptide (BNP; MIM 00295) and C-type natriuretic peptide (CNP; MIM 600296) [2]. NPR-A and NPR-B ligand binding affinities differ; ANP and BNP mainly bind NPR-A, CNP mainly binds NPR-B. NPR-C, the third and most abundantly expressed member of the natriuretic peptide receptor family, does not exert guanylyl cyclase action, instead it acts as a clearance receptor of natriuretic peptides (NPs). Local NP availability is partly regulated by NPR-C through internalization and degradation [3]. Additionally, activation of NPR-C may stimulate pertussis toxin–sensitive Gi binding domains that couple to adenyl cyclase inhibition and phospholipase activation [4].

Natriuretic peptide receptors and NPs have been implicated in various physiological processes, including longitudinal bone growth, energy metabolism, renal homeostasis, and cardiovascular regulation [2]. In particular, CNP and NPR-B are highly expressed in bone tissue, where the CNP/NPR-B signaling system acts as a paracrine mediator of the endochondral ossification process. NPR-B activation by CNP results in chondrocyte differentiation, hypertrophy, and

Received: 15 December 2021. **Editorial Decision:** 3 February 2022. **Corrected and Typeset:** 25 February 2022

extracellular matrix deposition. Consequently, dysfunction of the CNP/NPR-B signaling pathway may lead to aberrant longitudinal growth. For example, in transgenic mouse models, deletion of CNP and CNP overexpression led to dwarfism and overgrowth respectively [5, 6]. Human *NPR2* variants similarly cause a spectrum in phenotypical characteristics and variation in height [7]. Severe homozygous and compound heterozygous loss-of-function (LoF) variants lead to extreme short stature and skeletal dysplasia (acromesomelic dysplasia, Maroteaux type; MIM 602875) [8], while heterozygous LoF variants cause isolated mild short stature (MIM 616255) [9, 10]. On the other hand, heterozygous *NPR2* gain-of-function (GoF) variants lead to tall stature with arachnodactyly, macrodactyly of the halluces, pseudoepiphyses in hands and feet, coxa valga deformity with epiphyseal dysplasia and scoliosis (epiphyseal chondrodysplasia, Miura type; OMIM #615923) [11-14]. Overexpression of CNP due to chromosomal translocations causes a similar tall stature phenotype [15-17]. Homozygous and compound heterozygous LoF *NPR3* variants have recently been identified in individuals with tall stature, macrodactyly of the halluces, pseudo-epiphyses in hands and feet, and aortic root dilatation [18], reflecting the essential role of NPR-C in the regulation of CNP/NPR-B signal transduction and longitudinal bone growth.

Here we report on a boy with tall stature and macrodactyly of the halluces due to 2 novel compound heterozygous *NPR3* variants c.943G>A p.(Ala315Thr) and c.1294A>T p.(Ile432Phe), further broadening the phenotypic spectrum of NPR-C-related tall stature.

Methods

Patients

We studied a family of mixed Dutch and Surinamese origin, unrelated to the prior reported individuals with biallelic pathogenic variants in *NPR3* [18]. Blood samples were obtained from the proband, his parents, and his 2 younger sisters for genotyping, measurements of NPs and biochemical analyses. All family members aged 12 years and older signed informed consent forms. This study was approved by the medical ethical committee of Leiden, The Hague, and Delft (METC LDD).

Genetic Analysis

Genomic DNA of the probands was extracted from peripheral blood samples using the JANUS chemagic Pro Workstation (PerkinElmer, Waltham, MA, USA). Exomes were enriched with the Agilent Sureselect XT Human All Exon V5 kit (Agilent Technologies, Santa Clara, CA, USA) followed by Hiseq2500/4000 system sequencing (Illumina, San Diego, CA, USA). Coding sequences and flanking intron sequences of 56 genes associated with tall stature were analyzed with a stringent postsequencing annotation pipeline, consisting of BWA, GATK, and the custom-made variant filtering program LOVD3+ [19]. Genes included in the gene panel are given in Supplementary Table 1 [20]. Sanger sequencing was used for confirmation of identified variants in the proband and segregation analysis in family members. Primer sequences are available upon request.

In Silico Analysis of *NPR3* Variants

Several pathogenicity scores were used for analysis including PolyPhen-2 HumVar [21], CADD [22], Align GVGD [23], SIFT [24], and MutationTaster2 [25]. The DUET server (which incorporates the Mutation Cutoff Scanning Matrix [mCSM] and Site Directed Mutator [SDM] approaches) and DynaMut server were used to assess protein stability change [26, 27]. The ENCoM server was employed to assess protein flexibility change based on vibrational entropy [28]. The effects of residue substitution on important NPR-C structures, solvent accessibility, residue depth, interatomic interactions, and vibrational entropy energy were inspected with PyMOL (Schrödinger, Inc., USA). Crystal structure model 1JDN of NPR-C (doi:10.2210/pdb1JDN/pdb) was used for abovementioned analyses [29].

Biochemical Indices of Natriuretic Peptide Production/Clearance

Plasma measurements of CNP (RRID: AB_2904486; https://antibodyregistry.org/search.php?q=AB_2904486) [30], NTproCNP (RRID: AB_2904483; https://antibodyregistry.org/search.php?q=AB_2904483) [30], BNP (RRID: AB_518773; https://antibodyregistry.org/search?q=AB_518773) [31], ANP (RRID: AB_2904487; https://antibodyregistry.org/search?q=AB_2904487), and NTproANP (AB_519188) [32] were performed by radioimmunoassay in duplicate, as previously described, after extraction over C18 SepPac cartridges (Waters Corp, Milford, MA, USA). Intra- and inter assay coefficients of variations were as follows: CNP (5.0% and 8.5% at 8.1 pmol/L); NTproCNP (6.6% and 8.1% at 45 pmol/L); BNP (7.9% and 15.2% at 26 pmol/L); ANP (4.5% and 5.7% at 25.5 pmol/L); NTproANP (6.4% and 8.8% at 440 pmol/L). Plasma NTproBNP was assayed in singlicate by electrochemiluminescence immunoassay using the proBNP II assay on an automated Cobas e411 analyzer according to the manufacturer's instructions (Roche Diagnostics GmbH, Mannheim, Germany). Plasma and urine cGMP were measured after extraction over C18 SepPac cartridges by ELISA (cat. no. ADI-900-164, Enzo Life Sciences, Farmingdale, NY, USA; RRID: AB_290448; https://antibodyregistry.org/search?q=AB_2904485).

Construction of Expression Plasmids

The wild-type pEZ-M98 C-terminal GFP-tagged human *NPR3* (NM_000908) vector was purchased from GeneCopoeia (Tebu Bio, Heerhugowaard, the Netherlands). The different variants were introduced using the QuickChange site directed mutagenesis II kit (Agilent Technologies) according to the manufacturer's protocol. All vector constructs were verified by Sanger sequencing.

Cellular Localization Studies

Cellular localization experiments were performed using wild-type *NPR3*-GFP, p.(Ala315Thr) *NPR3*-GFP and p.(Ile432Phe) *NPR3*-GFP as previously described [18]. Additionally, HEK293T cells harboring the previously identified pathogenic variant p.(Ser148Pro) (p.(Ser148Pro) *NPR3*-GFP) were included as a positive control [18]. HEK293T cells were grown in DMEM medium supplemented with 10% FBS and 1% Pen/Strep (Gibco, San Diego, CA, USA). Cells were incubated at 37 °C in humidified air containing 5% CO_2. At 24 hours prior to transfection, cells were plated at a density of 1×10^5 cells/mL in 35 mm glass bottom dishes. Cells were transfected with Fugene 6 (Promega, Madison, WI, USA) according to manufacturer's instructions in a 6:1

ratio (Fugene 6:DNA). At 48 hours after transfection, cells were fixed with 4% formalin and washed with HBSS (Life Technologies, San Diego, CA, USA). Cell membranes were stained using Alexa Fluor wheat germ agglutinin (WGA) 555 (Thermo Fisher Scientific, Waltham, MA, USA). Vectashield Mounting medium containing 4′,6-diamidino-2-phenylindole (DAPI) (Vector Laboratories, Burlingame, CA, USA) was used to preserve fluorescence and to stain the nuclei. All high-resolution images were obtained using a Nikon Eclipse Ti-E inverted microscope attached to a microlens-enhanced dual spinning disk confocal system (UltraVIEW VoX; PerkinElmer) equipped with 405, 488, and 561 nm diode lasers for excitation of blue, green, and red fluorophores, respectively. A 60× magnification was used. Images were acquired and processed using Volocity 6.0.1 software (Improvision, PerkinElmer).

Results

Case Presentation

The proband, a 14-year-old boy, was referred by the general practitioner at age 10 years for evaluation of tall stature. He was born at term to nonconsanguineous parents after a normal pregnancy and delivery. At birth, his weight was 3860 g (+0.65 SDS) and length 53 cm (+1.24 SDS). Developmental milestones were attained at appropriate ages. General physical examination of heart, lungs, and abdomen was unremarkable. At age 10 years, his height was 172.1 cm (+3.67 SDS), weight for height –1.39 SDS, and head circumference was 56.5 cm (+1.73 SDS). Body proportions (sitting height to height ratio and arm span) were normal. Tanner stage was prepubertal. A radiograph of his left hand showed an advanced bone age of 11 years and 3 months at calendar age 10 years (assessed with the Greulich and Pyle atlas). No additional investigations were performed since predicted adult height was within the target height range (the expected final height based on parental heights). Target height was + 0.8 SDS, and target height range –0.8 to + 2.4 SDS. Follow-up controls were done with large intervals.

Percutaneous epiphysiodesis of both halluces (proximal and distal phalanx) was performed at age 12 years because of significantly longer halluces compared to the second digit (almost 2 cm) and European shoe size 47. At age 13 years, he was referred again to the orthopedic surgeon because of a predicted adult height of approximately 211 cm (+3.83 SDS). Pubertal progression was relatively slow and bone age was equal to calendar age at that time, resulting in a higher predicted adult height than before. Exome sequencing and targeted gene panel analysis of 56 genes associated with overgrowth was initiated (Supplementary Table 1 [20]). He underwent percutaneous epiphysiodesis of both knees at age 13.5 years (height 195.6 cm, +3.71 SDS), and osteotomia of the halluces during the same surgery because his halluces still kept growing. Pubertal development at that time was G5P5 with a testicular volume of 15 to 20 mL.

At physical evaluation at age 14 years, the proband had a height of 200 cm (+3.75 SDS). Sitting height to height ratio was 0.49 (–1.27 SDS), denoting relatively long legs despite percutaneous epiphysiodesis of both knees. Arm span was normal at 198.5 cm. He exhibited mild joint hypermobility as the Beighton score was 4. The 4 points were allocated because the "thumb sign" and "wrist sign" were positive on both sides, which could also be a sign of arachnodactyly (Fig. 1). Both thumbs were long, and both halluces were long and broad (Fig. 1). There were no other major dysmorphic features except for mild cutaneous syndactyly and a minor bilateral clinodactyly of the fifth finger, which was also present in his mother. Blood pressure was 111/69 mmHg, and heart rate 67 beats per minute. Radiographs of his feet and left hand demonstrated no bone abnormalities besides macrodactyly (longitudinally and circumferentially) of the halluces (Fig. 1). Notably, there were no pseudo-epiphyses visible. Cardiac evaluation revealed a normal aortic diameter (at the level of the sinus) and no heart abnormalities. At age 14.7 years, the proband's height was 205.1 cm (+3.93 SDS; Fig. 1). Weight was 73.9 kg and body mass index (BMI) 17.6 (–0.59 SDS).

His father of Surinamese descent (height 194.2 cm, +1.46 SDS compared to the Dutch background population) and his Dutch mother (height 175.2 cm, +0.71 SDS) did not show broad and long halluces, or any other aberrant clinical features including signs of skeletal dysplasia. Body proportions (sitting height to height ratio and arm span) of both parents were normal. The proband has 2 younger healthy sisters. The oldest sister had a height of 147.8 cm (–0.92 SDS) at age 11 years, and the youngest sister had a height of 151.2 (+0.92 SDS) at age 10 years. Both demonstrated heights within their target height range, and body proportions were normal. There were no aberrant clinical features at physical examination of the girls besides moderate generalized joint hypermobility (Beighton score 5/9).

At age 14.5 years the proband was admitted to a pediatric hospital with a pneumothorax after presenting to the emergency department because of progressive right-sided chest pain and dyspnea since a few weeks. Plain radiographs showed a collapsed lung and air in the right pleural space. A computed tomography scan of the lungs confirmed this and allowed identification of a pulmonary bleb of 1.3 cm in the apex of the right upper lobe, and 2 blebs of less than 1 cm in the apical zone of the left upper lobe. Lung parenchyma, tracheobronchial tree, and mediastinum (including aortic diameter) were normal. Based on the radiological examinations, the pneumothorax was classified as a primary simple spontaneous pneumothorax. An intercostal drain was inserted. He was discharged within 2 weeks; however, 3 days hereafter there was a recurrence of the right-sided pneumothorax. Video-assisted thoracoscopic surgery (VATS) was performed for right-sided pleurectomy and bullectomy. He recovered and radiographs showed no abnormalities at follow-up 2 months after surgery.

Identification of Heterozygous *NPR3* Variants

A gene panel consisting of genes responsible for tall stature and overgrowth syndromes (Supplementary Table 1 [20]) was used for filtering exome sequencing data. We identified 2 novel missense variants in *NPR3*: NM_001204375.1:c.943G>A, predicted to result in an alanine to threonine substitution at position 315 in exon 3, p.(Ala315Thr), and NM_001204375.1:c.1294A>T, predicted to result in an isoleucine to phenylalanine substitution at position 432 in exon 6, p.(Ile432Phe). Segregation analysis revealed that p.(Ala315Thr) was paternally inherited and p.(Ile432Phe) maternally inherited (Fig. 2). The proband's sisters both had biallelic wild-type *NPR3* alleles. Both *NPR3* missense variants have not been observed in Genome Aggregation Database or in-house control populations. The alanine residue at position 315 is fully conserved across multiple species, and NPR-A

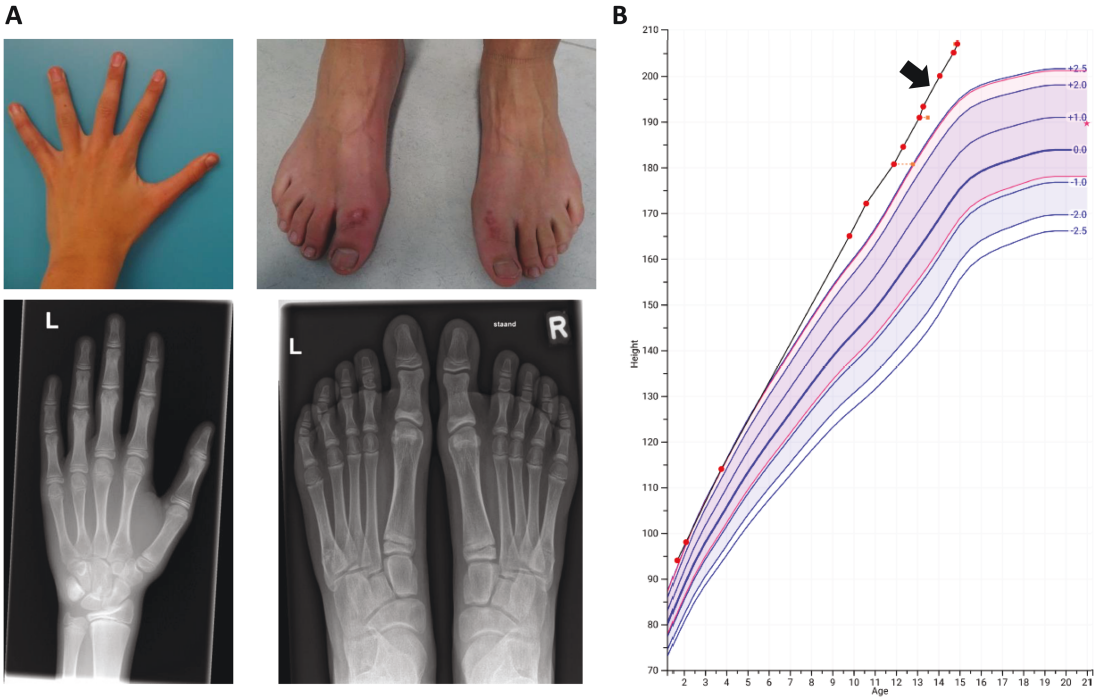

Figure 1. Photographs, radiographs, and growth curve of the proband. A, Photographs of left hand and feet were taken at age 14 years. The fingers are notable for arachnodactyly, mainly of the thumb, and mild cutaneous syndactyly. Both halluces show significant circumferential macrodactyly, despite epiphysiodesis, since only growth of longitudinal ossification centers may be accessed. Radiographs of the left hand and feet were taken at age 13 years and age 12 years respectively. Note that there are no pseudo-epiphyses present in the left hand and feet. B, Growth of the proband (black line and red dots) is compared to Dutch reference values for boys (blue area). From age 4 years there is a gradual growth acceleration from +2.5 SDS to +3.93 SDS at age 14.7 year. Epiphysiodesis of both knees was performed at age 13.5 years (black arrow). Growth velocity hereafter seems unchanged. Bone age (orange dot) at given calendar age (red dot). The red star and pink area represent target height and target height range, respectively.

and NPR-B (Fig. 3). Isoleucine at position 432 is conserved in some orthologous sequences; however, not across NPR-A and NPR-B (Fig. 3). These data suggest that both residues are important for proper NPR-C function and/or integrity.

Multiple pathogenicity scores indicated deleteriousness of the variants (Table 1). Also, both variants are predicted to alter protein stability and flexibility, based on DUET, DynaMut and ENCoM analyses (Table 1). Both *NPR3* variants are located in the extracellular domain of NPR-C. In silico structural analysis of the effect of both substitutions showed no perturbation of the NP binding pockets [33]. Residue relative solvent accessibility and residue depth were negligibly altered (data not shown). Both variants led to rigidification of the residue-surrounding area (Supplementary Fig. S1 [20]). While there were no steric clashes upon residue substitution, p.(Ala315Thr) resulted in 1 newly formed sidechain to sidechain hydrogen bond and 1 sidechain to main-chain carbonyl hydrogen bond, whereas p.(Ile432Phe) did not lead to a structural reorganization (Supplementary Figures S2 and S3 [20]). Based on these data, both variants most likely lead to increased degradation or trafficking defects due to abnormal folding of the protein.

Biochemical Indices of Natriuretic Peptide Production/Clearance, Energy Metabolism, and Bone Markers

To assess the effect of the *NPR3* variants on NP production and clearance, we determined NPs, their bio-inactive aminoterminal propeptides and plasma cGMP in the proband and his family members (Table 2). In the proband, NTproANP/ANP, NTproBNP/BNP, and NTproCNP/CNP ratios were below the reference interval, and plasma cGMP was elevated, supporting the hypothesis that both variants result in a reduced clearance by the mutated NPR-C receptor. Lower NTproANP/ANP and NTproBNP/BNP ratios in the proband's father could be interpreted as an effect of the stronger impact of the p.(Ala315Thr) variant. Interpreting biochemical indices of natriuretic peptide production/clearance in the unaffected sisters is hampered by insufficient knowledge on normal values in young girls (Table 2), rendering comparison with the proband complicated. The apparent higher ANP and BNP in sister 1 probably relate to the use of interquartile ranges and lack of a defined reference range at this age in girls—where levels are higher in girls than in boys.

When compared to the previously identified NPR-C LoF patients (Table 3), NTproANP/ANP and NTproCNP/CNP ratios are higher in the proband, while the NTproBNP/BNP ratio is noticeably lower. Considering this observation, it is important to point out that the NTproBNP assay used for the current study was the Roche Elecsys proBNP II assay. This assay reads lower than the NTproBNP RIA, which was used in the previous report on NPR-C LoF [18].

Since NPs are implicated in energy metabolism [38], and CNP is particularly implicated in longitudinal bone growth, we assessed indices of energy metabolism and bone markers in the proband and his first-degree relatives (Supplementary Table 2 [20]). Cholesterol, triglycerides, and apolipoprotein B-100 were lower than reference values in the proband, and the cholesterol/high-density lipoprotein ratio was lower

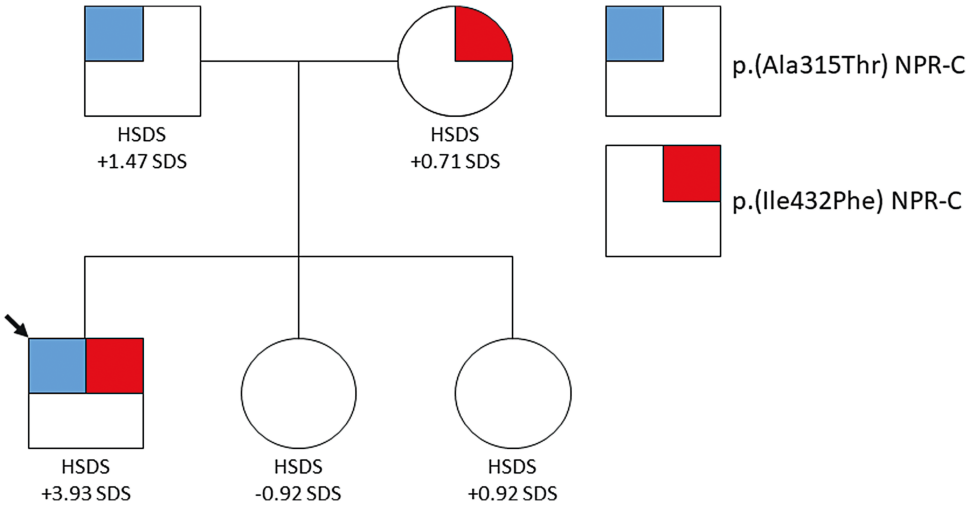

Figure 2. Pedigree.

```
                                                    ⬇
P17342_NPRC_HUMAN      291-  LFNSSSYGD------GSWKRGDK--HDFEAKQAYSSLQTVTLLRTVKPE -331
P70180_NPRC_MOUSE            LFNSSSYGD------GSWRRGDK--HDSEAKQAYSSLQTVTLLRTVKPE
P41740_NPRC_RAT              LFNSSSYGD------GSWKRGDK--HDFEAKQAYSSLQTVTLLRTAKPE
P10730_NPRC_BOVINE           LFNSSFYGD------GSWKRGDK--HDFEAKQAYSSLQTITLLRTVKPE
F1R7C4_NPRC_ZEBRAFISH        LFNSSSYGD------GSWRRRDK--YDDEARAAYSFLNTVTLLRSTKPE
E2R6Z0_NPRC_DOG              ------RGD------GSWKRGDK--HDFEAKQAYSSLQTITLLRTVKPE
M3W032_NPRC_CAT              LFNSSSYGD------GSWKRGDK--HDFEAKQAYSSLQTITLLRTVKPE
P16066_NPRA_HUMAN            IFGQSLQGGQGPAPRRPWERGDG--QDVSARQAFQAAKIITYKDPDNPE
P20594_NPRB_HUMAN            VFGESLRAGPTRATGRPWQDNRTREQAQALREAFQTVLVITYREPPNPE
                             ..        *.          : *:.    :*     :**

                                                    ⬇
P17342_NPRC_HUMAN      400-  IAGQVSIDANGDRYGDFSVIAMTDVEAGTQEVIGDYFGKEGRFEMRPNV -448
P70180_NPRC_MOUSE            IAGQVSIDANGDRYGDFSVVAMTDTEAGTQEVIGDYFGKEGRFQMRSNV
P41740_NPRC_RAT              IAGQVSIDANGDRYGDFSVVAMTDTEAGTQEVIGDYFGKEGRFKMRSNV
P10730_NPRC_BOVINE           IAGQVSIDANGDRYGDFSVIAMTDTEAGTQEVIGDYFGKEGRFEMRPNV
F1R7C4_NPRC_ZEBRAFISH        IAGQVSLDANGDRNGDFSVVRMTDPESGKHETVMNYFGTNGSFQILPGF
E2R6Z0_NPRC_DOG              IAGQVSIDANGDRYGDFSVIAMTDPEAGTQEVIGDYFGKEGRFEMRPNV
M3W032_NPRC_CAT              IAGQVSIDANGDRYGDFSVIAMTDPEAGTQEVIGDYFGKEGRFEMRPNV
P16066_NPRA_HUMAN            VTGYLKIDSSGDRETDFSLWDMDP-ENGAFRVVLNYNGTSQELVAVSGR
P20594_NPRB_HUMAN            VTGLVVMDKNNDRETDFVLWAMGDLDSGDFQPAAHYSGAEKQ-IWWTGR
                             ::* : :* ..**  ** :  *   : *  .   .* * .       .
```

Figure 3. Amino acid sequence alignment of residues 291-331 and 400-448 of NPR-C. Amino acid sequence alignments of the affected regions of NPR-C, compared with different orthologues, NPR-A and NPR-B. The black arrows indicate alanine at position 315 and isoleucine at position 432. Both regions show high sequence conservation across several species. Alanine at position 315 is also conserved in NPR-A and NPR-B. * Position with a single, fully conserved residue: Conservation between groups of strongly similar properties. Conservation between groups of weakly similar properties.

compared to his relatives. The bone markers P1NP (bone formation) and CTx (bone resorption) were within age- and sex-specific normal ranges, consistent with reported data in other affected individuals [18].

Cellular Localization of the p.(Ala315Thr) NPR-C Variant Is Cytoplasmic While the p.(Ile432Phe) NPR-C Variant Shows an Equivocal Cellular Distribution

Previously it was shown that the p.(Ser148Pro) and p.(Asp363Val) missense variants in *NPR3* resulted in aberrant cellular localization of the receptor [18]. Therefore, the cellular localization of the presently identified mutant receptor proteins was further investigated (Fig. 4). Localization studies using transfected HEK293T cells clearly demonstrated cytoplasmic retention of NPR-C harboring the p.(Ala315Thr) variant, possibly due to a trafficking defect. Cytoplasmic retention was also observed with HEK293T cells transfected with p.(Ile432Phe) but this was only partial, since some co-localization with the membrane marker was also present (Fig. 4). Accordingly, reduced membrane expression of NPR-C was more pronounced for the p.(Ala315Thr) variant, which substitutes the most conserved residue of the 2 variants, and was predicted to be more deleterious according to pathogenicity scores.

Discussion

Biallelic LoF variants in *NPR3* (encoding NPR-C) cause a tall stature phenotype associated with macrodactyly of the

Table 1. In silico analysis of identified *NPR3* variants

Prediction method	p.(Ala315Thr) score	p.(Ile432Phe) score
PolyPhen-2 (HumVar)	1.000 (probably damaging)	0.849 (possibly damaging)
CADD	31 (top 0.1% deleterious variants)	27.7 (top 1% deleterious variants)
SIFT	0 (deleterious)	0.01 (deleterious)
MutationTaster2	1 (disease causing)	1 (disease causing)
Align GVGD	C0 (least likely to interfere with function)	C0 (least likely to interfere with function)
DUET [a]	ΔΔG: -2.232 Kcal/mol (destabilizing)	ΔΔG: -1.579 Kcal/mol (destabilizing)
DynaMut [a]	ΔΔG: -0.950 kcal/mol (destabilizing)	ΔΔG: 0.237 kcal/mol(stabilizing)
ENCoM [a]	ΔΔSVib: -0.485 kcal mol^{-1} K^{-1} (decrease of flexibility)	ΔΔSVib: -0.641 kcal mol^{-1} K^{-1} (decrease of flexibility)

[a]A negative change in free Gibbs energy (ΔΔG) denotes a decrease of stability, which may lead to a wrongly folded protein and degradation in vivo. In ENCoM analyses ΔΔG is estimated by a change in vibrational entropy energy (ΔΔSVib).

halluces, a lean habitus, arachnodactyly, and sometimes aortic root dilatation [18]. NPR-C acts as clearance receptor of NPs, making it an important regulator of CNP/NPR-B signal transduction during endochondral ossification and tubular bone growth. Based on biochemical data, LoF of NPR-C presumably results in overactivation of NPR-B due to diminished clearance of CNP, which explains the highly similar phenotypes of NPR-B, CNP, and NPR-C-related tall stature. Here we report on a boy with extreme tall stature and macrodactyly of the halluces caused by 2 novel compound heterozygous *NPR3* variants c.943G>A p.(Ala315Thr) and c.1294A>T p.(Ile432Phe). In silico analysis of the variants indicated deleteriousness due to destabilizing properties of the amino acid substitutions. Biochemical indices of NP clearance in the proband demonstrated reduced NTproANP/ANP, NTproBNP/BNP, and NTproCNP/CNP ratios, consistent with NPR-C LoF. Functional analyses with transfected HEK293T cells showed that the identified variants result in reduced expression of NPR-C on the cell membrane, albeit there were differences between the variants in terms of degree of cell membrane expression. Based on these observations we conclude that the tall stature phenotype is likely caused by the biallelic *NPR3* variants.

Four probands with NPR-C-related tall stature were previously identified in 3 families [18]. All 4 probands had a reduced body weight to height ratio and pseudo-epiphyses in hands and feet, 3 had joint hypermobility and 2 unrelated probands had aortic root dilatation. We think the most likely explanation for absence of pseudo-epiphyses in hands and feet and aortic root dilatation in the current proband may be deduced from functional differences between *NPR3* variants of the proband and previous cases. Variant p.(Ile432Phe) appears to be less deleterious than p.(Ala315Thr) and the previously identified p.(Ser148Pro) since there was some co-localization of p.(Ile432Phe) NPR-C with the cell membrane (Fig. 4) as opposed to complete absence of NPR-C in the case of p.(Ala315Thr) and p.(Ser148Pro). Amino acid sequence alignment and in silico predictions corroborate the milder nature of p.(Ile432Phe) compared to p.(Ala315Thr) (Table 1, Fig. 3, Supplementary Figures S2 and S3 [20]). Also, whereas the height SDS and BMI reduction in the proband is largely similar to the previous cases [18], the NTproCNP/CNP ratio is less affected (Table 3), reflecting a milder biochemical profile. Presumably pseudo-epiphyses identified in the previously described 4 subjects result from more profound increases in CNP/NPR-C signaling and enhanced chondrocyte activity as reported in transgenic NPR-C LoF mice [39-41].

Reviewing growth patterns in affected individuals (all males, Supplementary Table 3 [20]), it seems that the increase in length at birth is modest, but height SDS increases progressively in later childhood. Similar patterns of growth acceleration later in childhood have been reported in skeletal overgrowth due to GoF of NPR-B [11, 14]. Conversely, subjects with NPR-B haploinsufficiency exhibit a relative and progressive loss of height velocity with age [42]. Collectively, these patterns suggest that an increase in intracellular CNP activity (due to either GoF of NPR-B or increase in CNP/NPR-B from LoF in NPR-C) reduces the rate of bone maturation, allowing a longer and more excessive growth phase during peripubertal years. During puberty, CNP increases due to the increase of sex steroids [43, 44], further delaying bone maturation and increasing height SDS. This hypothesis is consistent with evidence of reduced rates of bone maturation in experimental animals exhibiting LoF variants in NPR-C [39-41], and actions of exogenous CNP in CNP deficient rats [45]. Future serial study of bone and epiphyseal maturation, CNP, and growth are likely to clarify these relationships which could also provide insight to how CNP activity is regulated in mammals.

Results from biochemical analysis of NP production/clearance in the proband are comparable to the previous cases in showing lower values of bio-inactive/bioactive NP ratios for each of the 3 NPs [18]. Compared to his family members, each ratio is lower in the proband than in the unaffected siblings, and plasma cGMP is higher (Table 2). Across all reported cases (Table 3), ANP and CNP ratios were more perturbed in keeping with the higher affinity of ANP and CNP for NPR-C compared to BNP in humans [46]. Lack of evidence of suppression [47] of endogenous CNP (NTproCNP 0.24 SDS, Table 3) is consistent with the less deleterious genotype in the proband. However, these findings are subtle and using plasma concentrations of bioactive NP alone does not clearly distinguish the proband's disorder. Our ability to measure both bio-inactive (a measure of production) and bioactive forms (a measure of clearance) of NPs in subjects with overgrowth phenotypes enables the detection of NPR-C LoF in humans without recourse to tissue analyses; however, interpretation is context dependent.

Contrived genetic models of NPR-C LoF in mice, in addition to skeletal overgrowth, show cardio-renal abnormalities including excessive diuresis, plasma volume contraction, and hypotension mediated by NP/cGMP [40], or lower blood pressure associated with impaired renal tubular sodium reabsorption mediated by change in Gi/PLC/PKC pathway activity [48].

Table 2. Phenotype, NPs, and cGMP values in the proband and family members

	Proband	Father	Mother	Sib 1	Sib 2		
NPR3 genotype	A315T/I432F	A315T/wt	I432F/wt	wt/wt	wt/wt	Reference interval	
Age (sex)	14.7 (M)	43.6 (M)	47.2 (F)	12.3 (F)	10.8 (F)	Males	Females
Height SDS	+3.93	+1.46	+0.71	-0.92	+0.92		
ANP (pmol/L)	21.0	30.2	29.4	22.6	15.8	6.4–14 [a]	7.6–14 [a]
NTproANP (pmol/L)	285	490	541	416	346	247–406 [a]	305–506 [a]
NTproANP/ANP ratio	13.6	16.2	18.4	18.4	21.9	31–48 [a]	30–47 [a]
BNP (pmol/L)	10.7	9.8	14.2	8.9	5.9	2.8–4.5 [a]	3.3–5.9 [a]
NTproBNP (pmol/L)	2.0	1.8	18.4	6.6	3.3	0.9–3.8 [b]	2.2–7.4 [b]
NTproBNP/BNP ratio [c]	0.7	0.7	4.7	2.7	2.0	1.8–3.6[a]	2.7 – 4.3[a]
CNP (pmol/L) (SDS)	2.2 (0.94)	0.9 (1.77)	0.9 (0.94)	2.0 (0.7)	1.4 (-0.47)	1.4 – 2.1 [d]	1.2 – 2.0 [d]
NTproCNP (pmol/L) (SDS)	39.8 (0.24)	20.7 (0.98)	13.5 (-0.47)	46.2 (1.05)	37.2 (0.14)	29–44 [d]	29–41 [d]
NTproCNP/CNP ratio	18.5	23	15.5	23.1	27	20–27 [d]	19–28 [d]
Plasma cGMP (nmol/L)	5.1	4.6	2.0	4.4	3.1	0.2 – 2.8 [e]	0.2 – 2.8 [e]
Urine cGMP/cr ratio (mmol/mol)	51.4	50	35.8	66.1	76.6	48–103 [f]	48–103 [f]

Abbreviations: wt, wild-type; cr, creatinine.
[a]Adult reference interval (IQR) aged 50 years [34].
[b]Elecsys proBNP II Data Sheet reference interval (IQR) for individuals aged 40–49 years with no known cardiovascular disease.
[c]Conversion factor of 3.6 (unpublished comparative data) applied to the Elecsys proBNP II measurement.
[d]Childhood reference interval (IQR) for children aged 10-15 years [30]. Adult SDS were constructed with the LMS method on the basis of [35].
[e]Childhood reference values [36].
[f]Childhood reference interval (IQR) for children aged 10-14 years [37].

Table 3. Phenotype, NPs, and cGMP values in previously published subjects and the current proband with NPR-C LoF

	[18] Individual 1	[18] Individual 3	Current proband	
Age (years)	11	14	14.7	**Reference interval**
Sex	male	male	male	
Height SDS	+3.03	+3.9	+3.93	
BMI SDS	-2.3	-0.3	-0.59	
Blood pressure	99/62	95/54	111/69	
ANP (pmol/L)	33.7	24.4	21	6.4–14 [b]
NTproANP (pmol/L)	307	268	285	247–406 [b]
NTproANP/ANP ratio	9.1	11	13.6	31–48 [b]
BNP (pmol/L)	5.3	2.9	10.7	2.8–4.5 [b]
NTproBNP (pmol/L)	8.6	5.3	7.2 [a]	5.4–14 [b]
NTproBNP/BNP ratio	1.6	1.8	0.7 [a]	1.8–3.6[b]
CNP (pmol/L) (SDS)	2.5 (1.6 SDS)	6.8 (6.4 SDS)	2.2 (0.94 SDS)	1.4 – 2.1 [c]
NTproCNP (pmol/L) (SDS)	28.5 (-0.7 SDS)	37.4 (-0.05 SDS)	39.8 (0.24 SDS)	29–44 [c]
NTproCNP/CNP ratio	11.4	5.5	18.5	20–27 [c]
Plasma cGMP (nmol/L)	7.3	6.1	5.1	0.2 –2.8 [d]

[a]Conversion factor of 3.6 (unpublished comparative data) applied to the Elecsys proBNP II result to allow comparison with the Boudin cases 1 and 2 (measured by RIA).
[b]Adult male reference interval (IQR) aged 50 years [34].
[c]Childhood male reference interval (IQR) for children aged 10-15 years [30].
[d]Childhood reference values [36].

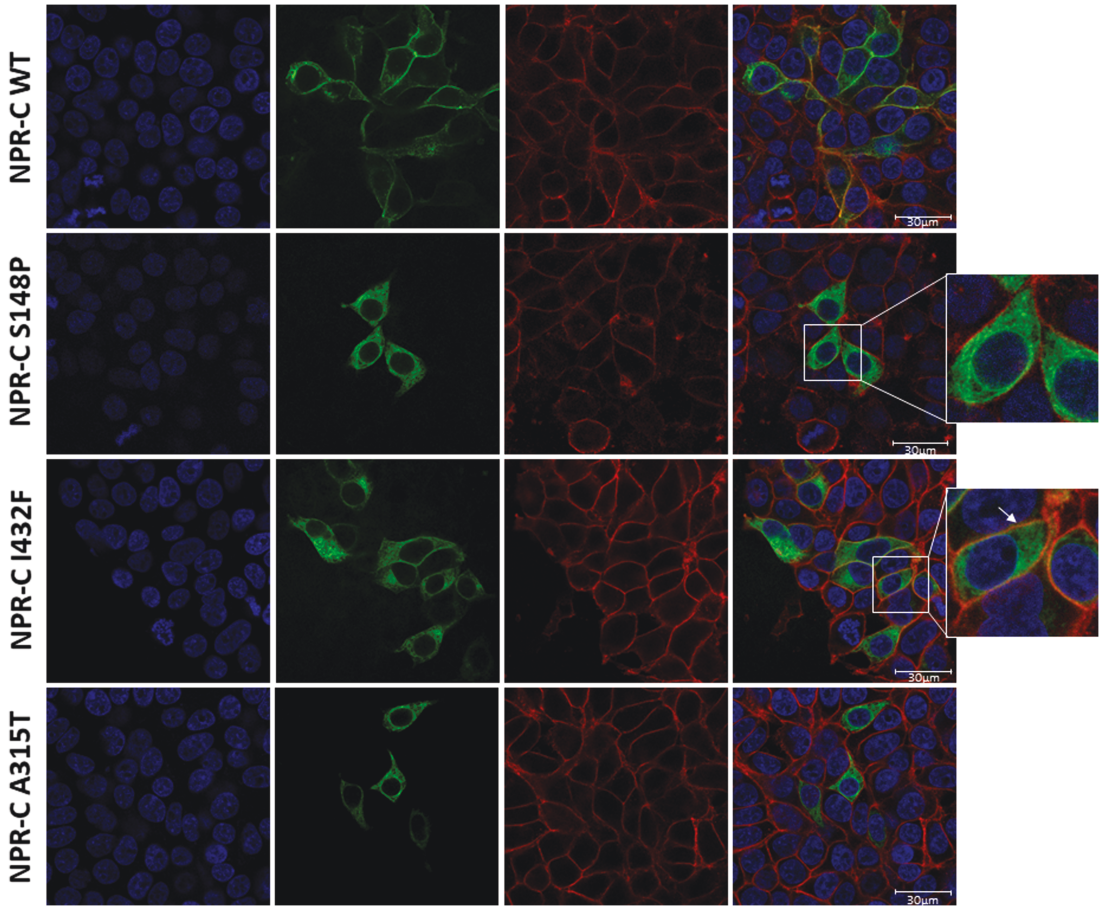

Figure 4. Mutant protein cellular localization. Comparison of NPR-C localization in HEK293T cells expressing wild-type and mutant *NPR3*-GFP. The p.(Ser148Pro) variant was previously identified in a patient with NPR-C LoF and serves as a positive control [18]. Nuclei are stained blue, cell membranes are marked red, and NPR-C carries a green label (GFP). The fourth column presents superimposed images. The wild-type receptor is expressed on the membrane, while p.(Ser148Pro) and p.(Ala315Thr) *NPR3*-GFP can only be observed in the cytoplasm. With regard to p.(Ile432Phe), both retention of the *NPR3*-GFP in the cytoplasm and co-localization of *NPR3*-GFP with the cell membrane (white arrow) can be observed.

In both studies, circulating concentrations of ANP and BNP were reduced. Notably, loss of ability to concentrate the urine was severe enough to raise hematocrit even in mice with monoallelic NPR-C LoF [40], although hypotension was only found in homozygotes. Increased urine cGMP in both heterozygote and homozygote mice was attributed to enhanced local concentrations of ANP/BNP in renal tissues. The present findings in the proband and obligatory carriers (the first to be reported in humans) show normal values of hematocrit, plasma creatinine, and GFR (Supplementary Table 2 [20]) with no evidence of volume contraction, hypotension, or history of excessive diuresis or natriuresis. Furthermore, while plasma cGMP is raised in the 3 affected subjects where the measurement was made, consistent with increased NP levels in plasma, urine excretion of cGMP indexed to creatinine was normal in the proband and in affected members of the current family (Table 2). These findings clearly differ from those in mice [40]. Whether humans with NPR-C LoF variants exhibit impaired sodium conservation, or hypotension when rendered volume depleted and the renin aldosterone axis is activated [48], are important issues requiring more focused studies.

The finding of a lean habitus and low value of lipids in the proband (Supplementary Table 2 [20]) aligns with findings of reduced weight/height ratios in the previous report [18] and NP actions on lipid and energy homeostasis [49, 50]. There is an inverse association between high NP levels and insulin insensitivity [34], yet homeostasis model assessment of insulin resistance (HOMA-IR) of the proband is comparable with siblings (Supplementary Table 2 [20]).

The proband has had 2 episodes of spontaneous pneumothorax associated with blebs, which has not been observed before in the context of abnormal CNP/NPR-B signaling. Blebs are frequently observed in otherwise healthy, young, thin, and/or tall individuals. However, blebs may also point at an underlying genetic condition such as Marfan syndrome. Sequencing did not identify a pathogenic variant in *FBN1*, there were no additional signs of a connective tissue disorder (eg, thin, translucent, fragile skin; aortic root dilatation), and thorax computed tomography revealed no signs of lung disease. We assume the pneumothorax was primarily caused by a ruptured bleb instigated by his tall stature and body habitus, secondary to NPR-C LoF. However, in light of the well-documented antifibrotic actions mediated by both NPR-A and NPR-B [2], and the antifibrotic effects of CNP in lung tissue [51], specific effects of the *NPR3* variants cannot be excluded.

In summary, with this report on a boy with tall stature and macrodactyly of the halluces, we further broaden the phenotypic spectrum of NPR-C-related tall stature. Our experiments indicate that the identified *NPR3* variants lead to NPR-C LoF, possibly due to decreased stability of NPR-C resulting in increased degradation or trafficking defects. An important clinical observation here is the absence of pseudoepiphyses of metacarpal and tarsal 1 and the middle and proximal phalanges in the hands and feet, and absence of aortic root dilatation, which could be indicative of a milder NPR-C LoF phenotype, as denoted by milder biochemical features of the proband compared to previous patients and an equivocal cellular distribution of p.(Ile432Phe) NPR-C. Finally, our data suggest that an increase in intracellular CNP activity reduces the rate of bone maturation, allowing a longer and more excessive growth phase during peripubertal years with subsequent underestimation of predicted adult height at a prepubertal age.

Acknowledgments

We are grateful for the participation of the proband and his family. We would like to thank Sander Spaans (Growth Analyser B.V., Rotterdam) for his help with constructing the growth curve depicted in Fig. 1. We would further like to thank Dr. Jeroen Corver (Department of Medical Microbiology, Leiden University Medical Center) for giving access to PyMOL.

Author Contributions

In vitro studies: E.B., W.H., G.M. Biochemical analysis of NPs: E.S., T.P. Genetic analysis: H.v.D., P.L. In silico analysis of *NPR3* variants: H.v.D, P.L. Gathering of clinical data: D.v.d.K, S.K., P.L. Writing of first draft: P.L., D.v.d.K., E.E., and H.v.D. Project coordination: H.v.D and G.M. All authors critically reviewed manuscript drafts and approved the final manuscript as submitted.

Grant Numbers

T.C.R.P. received a New Zealand Heart Foundation Senior Fellowship (grant number 1756).

E.B. received a postdoctoral grant of the research foundation Flanders (FWO Vlaanderen; grant number 12A3814N).

Statement of Ethics

The authors have no ethical conflicts to disclose. The proband and his family agreed to participate and signed informed consent.

Disclosures

The authors have no conflicts of interests to state. T.P. and E.E. have a patent titled “Assessment of skeletal growth using measurements of NT-CNP peptides”.

Data Availability

Variant data has been submitted to LOVD (http://www.lovd.nl/3.0/home). The datasets generated during and/or analyzed during the current study are not publicly available but are available from the corresponding author on reasonable request.

References

1. Potter LR, Yoder AR, Flora DR, Antos LK, Dickey DM. Natriuretic peptides: their structures, receptors, physiologic functions and therapeutic applications. *Handb Exp Pharmacol*. 2009(191):341-366. doi: 10.1007/978-3-540-68964-5_15
2. Kuhn M. Molecular physiology of membrane guanylyl cyclase receptors. *Physiol Rev*. 2016;96(2):751-804.
3. Potter LR. Natriuretic peptide metabolism, clearance and degradation. *FEBS J*. 2011;278(11):1808-1817.
4. Moyes AJ, Hobbs AJ. C-type natriuretic peptide: a multifaceted paracrine regulator in the heart and vasculature. *Int J Mol Sci*. 2019;20(9). doi: 10.3390/ijms20092281

5. Chusho H, Tamura N, Ogawa Y, *et al*. Dwarfism and early death in mice lacking C-type natriuretic peptide. *Proc Natl Acad Sci USA*. 2001;98(7):4016-4021.
6. Yasoda A, Komatsu Y, Chusho H, *et al*. Overexpression of CNP in chondrocytes rescues achondroplasia through a MAPK-dependent pathway. *Nat Med*. 2004;10(1):80-86.
7. Baron J, Savendahl L, De Luca F, *et al*. Short and tall stature: a new paradigm emerges. *Nat Rev Endocrinol*. 2015;11(12):735-746.
8. Bartels CF, Bukulmez H, Padayatti P, *et al*. Mutations in the transmembrane natriuretic peptide receptor NPR-B impair skeletal growth and cause acromesomelic dysplasia, type Maroteaux. *Am J Hum Genet*. 2004;75(1):27-34.
9. Vasques GA, Amano N, Docko AJ, *et al*. Heterozygous mutations in natriuretic peptide receptor-B (NPR2) gene as a cause of short stature in patients initially classified as idiopathic short stature. *J Clin Endocrinol Metab*. 2013;98(10):E1636-E1644.
10. Wang SR, Jacobsen CM, Carmichael H, *et al*. Heterozygous mutations in natriuretic peptide receptor-B (NPR2) gene as a cause of short stature. *Hum Mutat*. 2015;36(4):474-481.
11. Miura K, Namba N, Fujiwara M, *et al*. An overgrowth disorder associated with excessive production of cGMP due to a gain-of-function mutation of the natriuretic peptide receptor 2 gene. *PLoS One*. 2012;7(8):e42180.
12. Miura K, Kim OH, Lee HR, *et al*. Overgrowth syndrome associated with a gain-of-function mutation of the natriuretic peptide receptor 2 (NPR2) gene. *Am J Med Genet A*. 2014;164A(1):156-163.
13. Hannema SE, van Duyvenvoorde HA, Premsler T, *et al*. An activating mutation in the kinase homology domain of the natriuretic peptide receptor-2 causes extremely tall stature without skeletal deformities. *J Clin Endocrinol Metab*. 2013;98(12):E1988-E1998.
14. Lauffer P, Miranda-Laferte E, van Duyvenvoorde HA, *et al*. An activating deletion variant in the submembrane region of natriuretic peptide receptor-B causes tall stature. *J Clin Endocrinol Metab*. 2020;105(7). doi: 10.1210/clinem/dgaa190
15. Ko JM, Bae JS, Choi JS, *et al*. Skeletal overgrowth syndrome caused by overexpression of C-type natriuretic peptide in a girl with balanced chromosomal translocation, t(1;2)(q41;q37.1). *Am J Med Genet A*. 2015;167A(5):1033-1038.
16. Bocciardi R, Giorda R, Buttgereit J, *et al*. Overexpression of the C-type natriuretic peptide (CNP) is associated with overgrowth and bone anomalies in an individual with balanced t(2;7) translocation. *Hum Mutat*. 2007;28(7):724-731.
17. Moncla A, Missirian C, Cacciagli P, *et al*. cluster of translocation breakpoints in 2q37 is associated with overexpression of NPPC in patients with a similar overgrowth phenotype. *Hum Mutat*. 2007;28(12):1183-1188.
18. Boudin E, de Jong TR, Prickett TCR, *et al*. Bi-allelic loss-of-function mutations in the NPR-C receptor result in enhanced growth and connective tissue abnormalities. *Am J Hum Genet*. 2018;103(2):288-295.
19. Fokkema IF, Taschner PE, Schaafsma GC, Celli J, Laros JF, den Dunnen JT. LOVD v.2.0: the next generation in gene variant databases. *Hum Mutat*. 2011;32(5):557-563.
20. Lauffer P, Boudin E, van der Kaay DCM, *et al*. Supplementary Files from: Broadening the spectrum of loss-of-function variants in NPR-C-related extreme tall stature. Posted February 1, 2022. https://figshare.com/articles/dataset/Supplemental_Files_from_Tall_stature_and_macrodactyly_of_the_halluces_due_to_biallelic_loss-of-function_variants_in_natriuretic_peptide_receptor-C/17091203
21. Adzhubei IA, Schmidt S, Peshkin L, *et al*. A method and server for predicting damaging missense mutations. *Nat Methods*. 2010;7(4):248-249.
22. Kircher M, Witten DM, Jain P, O'Roak BJ, Cooper GM, Shendure J. A general framework for estimating the relative pathogenicity of human genetic variants. *Nat Genet*. 2014;46(3):310-315.
23. Tavtigian SV, Deffenbaugh AM, Yin L, *et al*. Comprehensive statistical study of 452 BRCA1 missense substitutions with classification of eight recurrent substitutions as neutral. *J Med Genet*. 2006;43(4):295-305.
24. Vaser R, Adusumalli S, Leng SN, Sikic M, Ng PC. SIFT missense predictions for genomes. *Nat Protoc*. 2016;11(1):1-9.
25. Schwarz JM, Cooper DN, Schuelke M, Seelow D. MutationTaster2: mutation prediction for the deep-sequencing age. *Nat Methods*. 2014;11(4):361-362.
26. Rodrigues CH, Pires DE, Ascher DB. DynaMut: predicting the impact of mutations on protein conformation, flexibility and stability. *Nucleic Acids Res*. 2018;46(W1):W350-W355.
27. Pires DE, Ascher DB, Blundell TL. DUET: a server for predicting effects of mutations on protein stability using an integrated computational approach. *Nucleic Acids Res*. 2014;42(Web Server issue):W314-W319.
28. Frappier V, Najmanovich RJ. A coarse-grained elastic network atom contact model and its use in the simulation of protein dynamics and the prediction of the effect of mutations. *PLoS Comput Biol*. 2014;10(4):e1003569.
29. He X, Chow D, Martick MM, Garcia KC. Allosteric activation of a spring-loaded natriuretic peptide receptor dimer by hormone. *Science*. 2001;293(5535):1657-1662.
30. Olney RC, Permuy JW, Prickett TC, Han JC, Espiner EA. Amino-terminal propeptide of C-type natriuretic peptide (NTproCNP) predicts height velocity in healthy children. *Clin Endocrinol (Oxf)*. 2012;77(3):416-422.
31. Palmer SC, Prickett TC, Espiner EA, Yandle TG, Richards AM. Regional release and clearance of C-type natriuretic peptides in the human circulation and relation to cardiac function. *Hypertension*. 2009;54(3):612-618.
32. Yandle TG, Espiner EA, Nicholls MG, Duff H. Radioimmunoassay and characterization of atrial natriuretic peptide in human plasma. *J Clin Endocrinol Metab*. 1986;63(1):72-79.
33. He XL, Dukkipati A, Garcia KC. Structural determinants of natriuretic peptide receptor specificity and degeneracy. *J Mol Biol*. 2006;361(4):698-714.
34. Prickett TCR, Spittlehouse JK, Miller AL, *et al*. Contrasting signals of cardiovascular health among natriuretic peptides in subjects without heart disease. *Sci Rep*. 2019;9(1):12108.
35. Prickett TCR, Olney RC, Cameron VA, Ellis MJ, Richards AM, Espiner EA. Impact of age, phenotype and cardio-renal function on plasma C-type and B-type natriuretic peptide forms in an adult population. *Clin Endocrinol (Oxf)*. 2013;78(5):783-789.
36. Weil J, Gerzer R, Strom T, *et al*. Increased plasma cyclic guanosine monophosphate concentrations in children with high levels of circulating atrial natriuretic peptide. *Pediatrics*. 1987;80(4):545-548.
37. Murad F, Moss WW, Johanson J, Selden RF. Urinary excretion of adenosine 3',5'-monophosphate and guanosine 3',5'-monophosphate in normal children and those with cystic fibrosis. *J Clin Endocrinol Metab*. 1975;40(4):552-559.
38. Wu W, Shi F, Liu D, *et al*. Enhancing natriuretic peptide signaling in adipose tissue, but not in muscle, protects against diet-induced obesity and insulin resistance. *Sci Signal*. 2017;10(489). doi: 10.1126/scisignal.aam6870
39. Jaubert J, Jaubert F, Martin N, *et al*. Three new allelic mouse mutations that cause skeletal overgrowth involve the natriuretic peptide receptor C gene (Npr3). *Proc Natl Acad Sci USA*. 1999;96(18):10278-10283.
40. Matsukawa N, Grzesik WJ, Takahashi N, *et al*. The natriuretic peptide clearance receptor locally modulates the physiological effects of the natriuretic peptide system. *Proc Natl Acad Sci USA*. 1999;96(13):7403-7408.
41. Esapa CT, Piret SE, Nesbit MA, *et al*. Mice with an N-Ethyl-N-Nitrosourea (ENU) induced Tyr209Asn mutation in natriuretic peptide receptor 3 (NPR3) provide a model for kyphosis associated with activation of the MAPK signaling pathway. *PLoS One*. 2016;11(12):e0167916.
42. Hanley PC, Kanwar HS, Martineau C, Levine MA. Short stature is progressive in patients with heterozygous NPR2 mutations. *J Clin Endocrinol Metab*. 2020;105(10). doi: 10.1210/clinem/dgaa491
43. Olney RC, Prickett TC, Yandle TG, Espiner EA, Han JC, Mauras N. Amino-terminal propeptide of C-type natriuretic peptide and linear

growth in children: effects of puberty, testosterone, and growth hormone. *J Clin Endocrinol Metab*. 2007;92(11):4294-4298.
44. Prickett TCR, Barrell GK, Wellby M, Yandle TG, Richards AM, Espiner EA. Effect of sex steroids on plasma C-type natriuretic peptide forms: stimulation by oestradiol in lambs and adult sheep. *J Endocrinol*. 2008;199(3):481-487.
45. Hirota K, Furuya M, Morozumi N, *et al*. Exogenous C-type natriuretic peptide restores normal growth and prevents early growth plate closure in its deficient rats. *PLoS One*. 2018;13(9): e0204172.
46. Mukoyama M, Nakao K, Hosoda K, *et al*. Brain natriuretic peptide as a novel cardiac hormone in humans. Evidence for an exquisite dual natriuretic peptide system, atrial natriuretic peptide and brain natriuretic peptide. *J Clin Invest*. 1991;87(4): 1402-1412.
47. Espiner E, Prickett T, Olney R. Plasma C-type natriuretic peptide: emerging applications in disorders of skeletal growth. *Horm Res Paediatr*. 2018;90(6):345-357.
48. Shao S, Li X-D, Lu Y-Y, *et al*. Renal natriuretic peptide receptor-C deficiency attenuates NaCl cotransporter activity in angiotensin II–induced hypertension. *Hypertension*. 2021. doi:10.1161/HYPERTENSIONAHA.120.15636.
49. Coué M, Moro C. Natriuretic peptide control of energy balance and glucose homeostasis. *Biochimie*. 2016;124:84-91.
50. Coué M, Barquissau V, Morigny P, *et al*. Natriuretic peptides promote glucose uptake in a cGMP-dependent manner in human adipocytes. *Sci Rep*. 2018;8(1):1097.
51. Kimura T, Nojiri T, Hino J, *et al*. C-type natriuretic peptide ameliorates pulmonary fibrosis by acting on lung fibroblasts in mice. *Respir Res*. 2016;17:19.